International Forum on Aeroelasticity and Structural Dynamics
IFASD 2024
17-21 June 2024, The Hague, The Netherlands

LINEARIZED CFD AND CSM BASED FLUTTER PROCESS FOR VERY FLEXIBLE AIRCRAFT

Bernd Stickan[1], Theo Meyer[1], Reik Thormann[1], Michael Wrightson[1], Alfonso Velencoso Gomez[1], Paolo Mastracci[2], Thomas Wilson[3]

[1]Airbus Operations GmbH
Airbus-Allee 1, 28199 Bremen, Germany

[2]Airbus Operations Ltd.,
Bristol, BS34 7QQ, United Kingdom

[3]Airbus UpNext.,
Bristol, BS34 7QQ, United Kingdom

Keywords: structural dynamics, aeroelasticity, Linearized CFD, LFD, flutter analysis, ROM, nonlinear CSM

Abstract:

This paper proposes a method to combine dynamic aerodynamic and structural data at different steady conditions to allow a p-k-based flutter process for constant mass and Mach. The full aircraft application case with aspect ratio 17 is used to show the relevance of mass- and altitude-dependent unsteady aerodynamics, but it also shows that for a relatively flexible wing nonlinear structural effects cannot be neglected. For the aerodynamic modelling, linearised RANS CFD aerodynamics are used. A detailed FEM is employed for structural modelling, which is deformed according to the steady conditions to cover geometric nonlinearities in the flutter process.

1 INTRODUCTION

New aircraft developments might include higher aspect ratio wings compared to the current commercial transport aircraft. Their aspect ratio is currently around nine, whereas new studies, like truss-braced wings, see [1], envisage an aspect ratio between 15 and 19. To reduce the mass penalty for such designs, these wings will usually become more flexible. It has already been shown by many authors, e.g. [2] and [3] that for a more flexible wing the consideration of structural geometric nonlinearities cannot be neglected for flutter studies. Furthermore, considering flutter analysis with constant mass and Mach-number, not only the structural parameters change along the airspeed/altitude axis, but also the unsteady aerodynamics change strongly due to varying angle of attack and wing deformation, see in [4].

While often linear flutter analysis is performed in the aircraft's jig-shape with flow-condition independent panel-method aerodynamics, in the following studies the structural model but also the CFD-based aerodynamics should be linearised around the accurate flight condition. This means, the modal mass and stiffness matrix as well as the mode shapes themselves and the resulting unsteady aerodynamics become dependent on the static aeroelastic equilibrium state and therefore, the challenges for flutter stability analysis are increased compared to a purely linear analysis.

To not miss important effects for this study, a detailed structural model including all control surfaces and linearised Reynolds-Averaged Navier-Stokes (RANS) aerodynamics are used. Since this leads to quite high computational costs if for each data-point of the p-k-method new CFD aerodynamics were computed, the p-k method is updated so that within the p-k solver it is interpolated between a set of data points. Each data point is a set of generalised stiffness, mass and aerodynamic matrices.

The application case for this paper is an aircraft with aspect ratio 17 and a wing deformation of up to 13% relative to half-wing-span. It is designed for transonic Mach numbers.

2 METHODS

2.1 Equations of Motion

The generalised equations of motion

$$\mathbf{M}\ddot{\mathbf{q}} + \mathbf{D}\dot{\mathbf{q}} + \mathbf{K}\mathbf{q} = \mathbf{\Phi}_\mathbf{s}^\mathbf{T}\mathbf{f}_\mathbf{s}, \tag{1}$$

including the mass matrix $\mathbf{M}$, the damping matrix $\mathbf{D}$, stiffness matrix $\mathbf{K}$, the modal coordinate $\mathbf{q}$ and generalised applied forces as product of mode-shape matrix $\mathbf{\Phi_s}$ and forces $\mathbf{f_s}$. This equation is transferred to the frequency domain to achieve the classical flutter equation:

$$\left[\left(p\frac{v_\infty}{c_{ref}}\right)^2\mathbf{M} + p\frac{v_\infty}{c_{ref}}\mathbf{D} + \mathbf{K} - q_\infty\mathbf{GAF}\left(k\right)\right]\cdot\mathbf{q} = 0\,. \tag{2}$$

q_∞ denotes the dynamic reference pressure. The frequency domain stability boundaries are computed by applying the classical p-k-method to the frequency-domain equation, see [5].

Here the important differences to classical flutter analysis is that, if an altitude/velocity dependent flutter loop is performed in the nonlinear sense, the mass matrix $\mathbf{M}$, stiffness matrix $\mathbf{K}$ and generalised air force matrix$\mathbf{GAF}$ depend on q_∞ or v_∞, too. So in this case the equation can be defined like

$$\left[\left(p\frac{v_\infty}{c_{ref}}\right)^2\mathbf{M}\left(v_\infty\right) + p\frac{v_\infty}{c_{ref}}\mathbf{D} + \mathbf{K}\left(v_\infty\right) - q_\infty\mathbf{GAF}\left(k, v_\infty\right)\right]\cdot\mathbf{q} = 0\,. \tag{3}$$

These airspeed dependent matrices are computed upfront for different flight conditions and then interpolated via first- or second-order spline in the p-k-method. This approach has the difficulty that the eigenmodes in $\mathbf{\Phi}$ change their shape, but also the mode order may differ for different q_∞ since the structural model deforms differently. It can even happen that modes at one flight condition cannot be found for other flight conditions. For this purpose a mode-mapping method based on the MAC value is created. Therefore, structural and aerodynamic matrices are mapped to the first flight condition. Modes which do not exist for all flight conditions are neglected.

2.2 Structural Modelling

MSC NASTRAN is used to perform the eigenmode analysis. The resulting generalised mass and stiffness matrix is used for the subsequent computations. To introduce the dependency on the flight condition, the FEM is deformed with the same beam coupling which is used for the steady CFD surface mesh deformation. In this manner geometric nonlinearities are introduced into the structural modelling. To enable this approach, all mechanical orientation (e.g. material

orientation) had to be modified to a mesh-grid dependent orientation. This has the advantage that the mechanical orientation is dependant only on the mesh grid position and therefore it is automatically updated once the mesh is deformed. Furthermore, lumped masses must be moved and the moments of inertia must be rotated. A similar way of working was followed in [3]. An exemplary plot of such deformed and undeformed FEM can be observed in Figure 1. Doubtless, a nonlinear solution sequence would be preferable, but this specific FEM was not suitable for this. The method was verified with a beam-representation of the structure for the low frequency modes in Section 5.1.

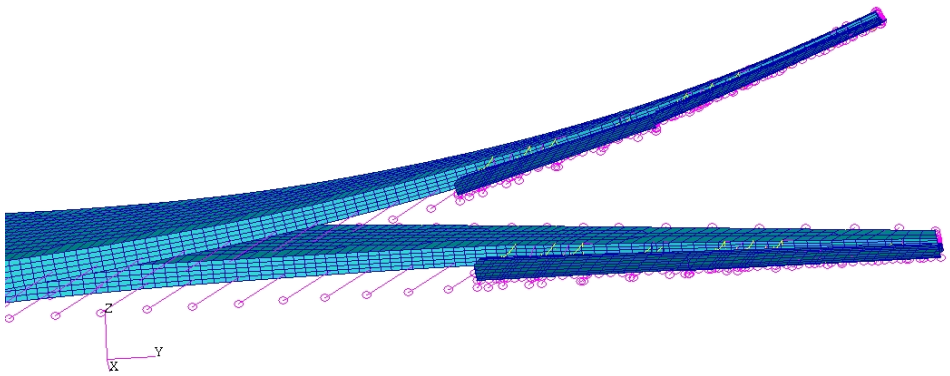

Figure 1: Undeformed and deformed structural model, wing-view, application example

2.3 Fluid-Structure Coupling

With the coupling method presented in Section [4] the structural displacements $\mathbf{d_s}$ are interpolated to the CFD surface mesh to get the aerodynamic surface displacements $\mathbf{d_a}$. The aerodynamic forces $\mathbf{f_a}$ are transferred to the structural model with a nearest-neighbour mapping to get the structural forces $\mathbf{f_s}$. Additionally, the same coupling method is used interpolate the structural eigenmodes $\mathbf{\Phi_s}$ to the aerodynamic surface to get $\mathbf{\Phi_a}$. For the steady CFD-CSM computation a correction method is used to keep the wing-length constant.

2.4 Aerodynamics

The linearised CFD code TAU by the DLR is used to compute the steady pressure coefficients $\mathbf{cp}$ and the unsteady pressure coefficient transfer functions $\mathbf{\hat{cp}}$ for different structural eigenmodes $\mathbf{\Phi_i}$. The solver is working with a cell-vertex-based finite volume scheme on unstructured grids. In the following studies the Spalart-Allmaras turbulence model is used. The computation of the unsteady pressures $\mathbf{\hat{cp}}$ uses the linearized variant of TAU, the so-called Linearized Frequency Domain (LFD) solver. This is strongly reducing the computation time for the needed data points. For more details see [6].

As preprocessing step for the LFD computation the surface mesh modes $\mathbf{\Phi_a}$ are transferred to the volume mesh via radial basis function interpolation plus nearwall-correction method, see [7] and [4]. The same method is used also for the CFD-deformation during the static CFD-CSM loop.

The steady pressures $\mathbf{cp}$, the unsteady pressures $\mathbf{\hat{cp}}$ and the surface normal derivative $\mathbf{\hat{n}}$ are used to compute the GAF matrix entries for different frequencies, resulting in a three-dimensional GAF matrix G of size nExcitationModes X nInfluencedModes X nFrequencies. Each entry is

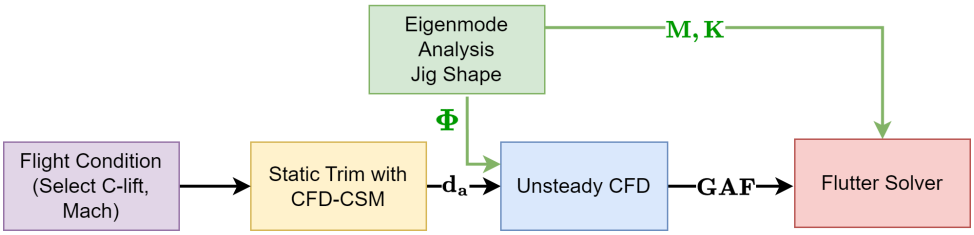

Figure 2: Flutter process 1 (FP1) for constant lift coefficient, linear structure

computed by

$$\mathrm{GAF}_{\mathrm{i,j,k}} = \mathbf{\Phi}_{\mathrm{j}}^{\mathrm{a,T}} \left(\hat{\mathbf{cp}}_{\mathrm{i,k}} \cdot \mathbf{n} \cdot \mathbf{A} + \mathbf{cp} \cdot \frac{\mathbf{d}\left(\mathbf{n} \cdot \mathbf{A}\right)}{\mathbf{dq_i}} \right), \tag{4}$$

whereas $\mathbf{\Phi}_{\mathrm{j}}^{\mathrm{a,T}}$ is the j-th mode-shape, $\hat{\mathbf{cp}}_{\mathrm{i,k}}$ the unsteady pressure transfer function of mode i at frequency k, n the surface normal matrix and A the surface cell area vector. $\frac{\mathbf{d(nA)}}{\mathbf{dq_i}}$ is the surface normal and cell area derivative for mode i.

3 FLUTTER PROCESS DESCRIPTIONS

Three different flutter processes are compared in the result section. The three flutter processes are named FP1, FP2 and FP3.

3.1 FP1: Constant Lift Coefficient

The first process is the most classical, which is only correct for one C-lift value of the aircraft and for a very rigid structure. Figure 2 shows the process in detail. It starts with the selection of the flight condition. Since the process tries to cover the complete speed/altitude range of flutter computation with only one unsteady aerodynamic model, the most conservative flight conditions should be selected. For this condition a static trim with CFD-CSM is performed to compute the flight shape. The structural model in Jig-shape is used to compute eigenmodes which are used for the creation of the unsteady aerodynamic model in the computed flight shape. Finally, stiffness $\mathbf{K}$, mass $\mathbf{M}$ and GAF matrix are fed into the flutter solver. The damping matrix $\mathbf{D}$ is neglected in this and the following sketches. A constant structural damping is used for all modes. It is clear that the assumption of constant lift coefficient and rigid structure is not valid, especially for a high aspect ratio wing.

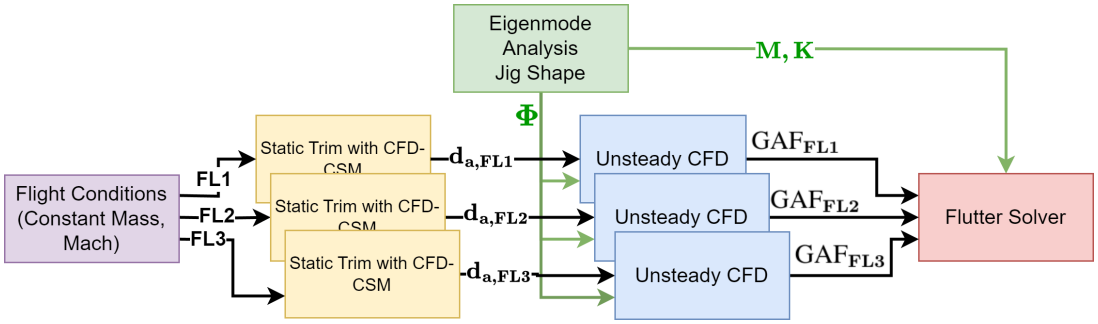

Figure 3: Flutter process 2 (FP2) for constant mass, linear structure

3.2 FP2: Constant Mass with Linear Structure

The second flutter process shown in Figure 3 increases the fidelity level by using more than one aerodynamic linearisation point, depicted here for three points. The different linearisation points have the aircraft mass and the Mach-number in common, but the altitude (flight level

=FL) is different. Hence the indices $FL1$, $FL2$, $FL3$ are used. Now for each flight level a static trim with CFD-CSM is performed. Then the same jig-shape modes are used to compute an unsteady aerodynamic model for each flight level. In the flutter solver, which performs a solution sequence starting at zero-speed up to the desired final speed value step by step, the aerodynamic $\mathrm{GAF_i}$ matrices are interpolated according to the current speed which correlates to the flight-level via the standard atmosphere.

3.3 FP3: Constant Mass with Nonlinear Structure

The third flutter process presented in Figure 4 increases fidelity by taking into account geometric nonlinearities of the structural model. In this process the structural model is deformed for each flight level and the eigenmode analysis is performed in the deformed shape. The computation of the unsteady aerodynamic model for each flight level is taking the different mode shapes $\mathbf{\Phi_i}$ at each flight level into account. But the aerodynamic linearisation point, the angle of attack and wing-deformation is equal to flutter process 2 (FP2). The deformed CSM is not pre-loaded for the following studies. A small pre-loading study has shown only a small influence. [3] does show only margninal influence of pre-loading, too.

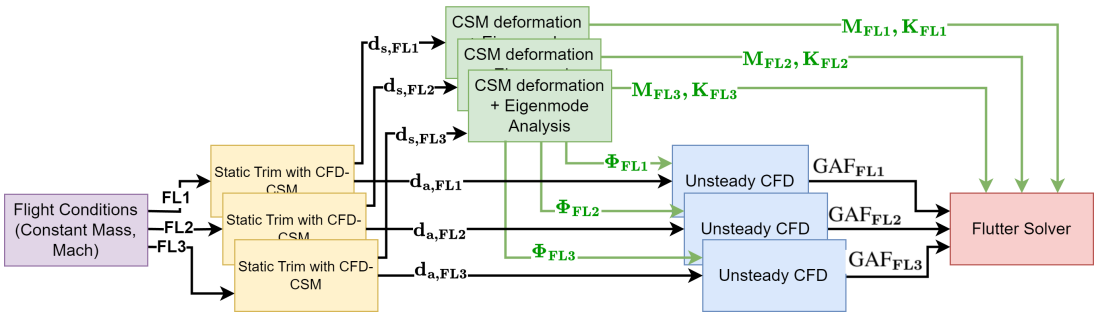

Figure 4: Flutter process 3 (FP3) for constant mass, structure covering geometric nonlinearities

4 CSM AND CFD MODELLING

As already mentioned in the previous section, a detailed structural model is used for the following investigations. It contains around 2 million elements of beam to volume types. For the aerodynamic modelling a relatively coarse CFD mesh of around 7 million nodes is used. But past flutter mesh convergence studies in [8] have shown that such mesh should be sufficiently accurate for the following studies.

5 RESULTS

5.1 CSM Solver External Geometric Nonlinear Modelling Validation

Two steps have been performed to validate the sequence of detailed CSM deformation (without nonlinear NASTRAN solution) and subsequent modal analysis with NASTRAN. The first step was to rotate the complete CSM model rigidly. In this case, the resulting eigenfrequencies differ around 0.5%. This indicates that the CSM deformation procedure is working well, but not perfect. Certain element types might need further investigation to perform the right rotation.

As a second step a beam-type CSM has been created from the detailed structural model. This model without control surfaces could be used for a nonlinear solution sequence in NASTRAN (SOL 400) of static deformation and subsequent modal analysis. The mean difference between detailed CSM and beam CSM in frequency for the first 25 modes is around 0.15 percent. The mean MAC values of the two model mode shapes is around 98.5 %. The plot in Figure 5 shows

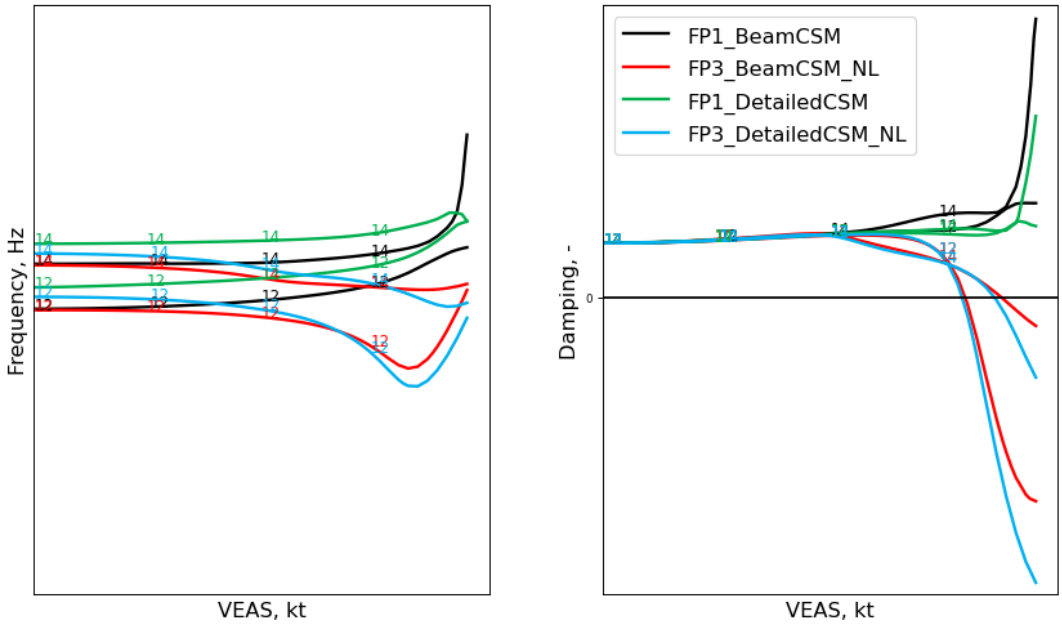

Figure 5: Comparison of beam-type and detailed CSM model for flutter process FP1 and FP3 for only one flight level

that for two geometrically very sensitive low frequency modes the two modelling approaches show quite similar results.

-	wing-tip-deformation in %-half-span			angle of attack		
Mach-number	FL1	FL2	FL3	FL1	FL2	FL3
Low	7.02	8.26	9.17	0.76	1.23	2.65
Low, 1.7G	9.98	11.62	13.18	1.84	2.73	5.35
Medium	6.30	9.46	9.26	0.50	0.91	2.12
High	6.17	7.94	9.12	0.58	0.97	2.42

Table 1: CFD-CSM trim wing-tip deformation and angle of attack for different flight conditions (Flight-levels for different Mach-numbers not equal!)

Coupling number	Description
10	3-node wing-bending
16	3-node wing in-plane
30	6-nnode wing-bending
35	7-node wing-bending

Table 2: Complex flutter coupling/mode descriptions, valid for all flutter plots

5.2 Linear CSM and GAF Interpolation

In this section the focus is on the flutter process 2 (FP2) in which the GAF-matrix only is interpolated. For this purpose 3 aerodynamic models were computed at different flight levels for 3 different Mach-numbers. The steady deformation amplitude of the wing-tip and the angle of attack can be observed in Table 1. It shows for the different flight levels (which are not equal

for the different Mach-numbers) the resulting wing-tip deformation and the angle of attack. It can be observed that the angle of attack varies strongly and therefore the steady aerodynamics are quite different. This has a direct impact on the unsteady aerodynamics.

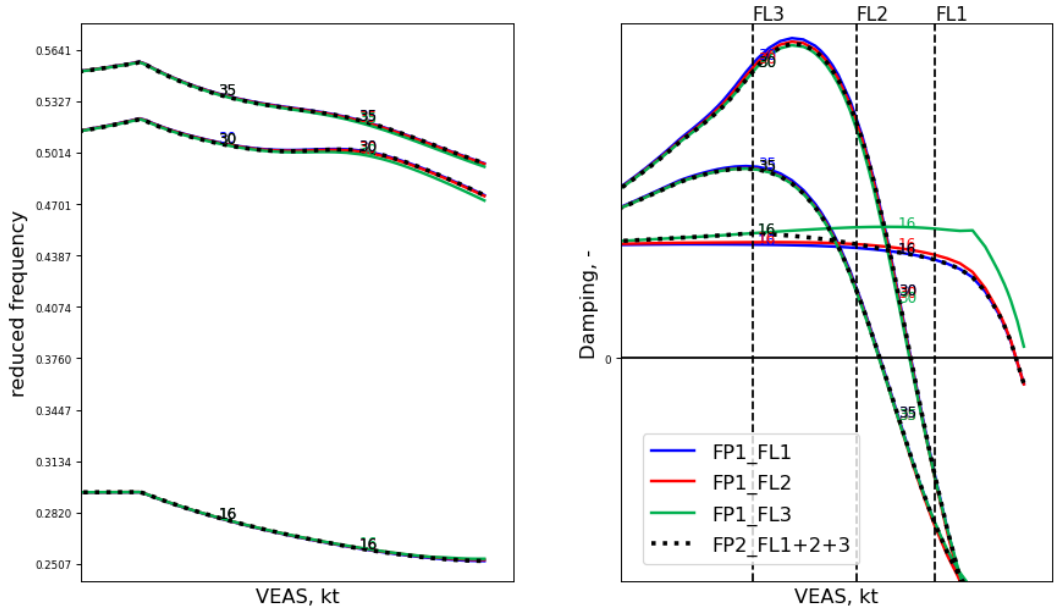

Figure 6: Flutter results flutter process (FP) 1+2 for lower Mach-number: Linear CSM, FP1 for 3 flight levels (FL), FP2 with GAF interpolation of same GAF data

Since in this section FP1 + FP2 are followed, the modes for the unsteady CFD and GAF computation depend on the same modes, computed in the jig-shape. In Figure 6 it can be observed that the resulting frequency and damping curves do not change strongly between the flight-levels for the low Mach-number. The differences increase if the target lift is increased to a 1.7G case (lift coefficient increased by factor 1.7). In Figure 7 the results are depicted. It can be noted that the FP2-curve crosses as expected the FP1-curves at the flight-level lines. Since no extrapolation is activated, in front of flight-level 3 and behind flight-level 1 the according curves lie on top of each other. The different presented flutter couplings are described in Table 2. The table is valid for all cases.

The two higher Mach-numbers in Figure 8 and 9 show strongly increasing differences. Due to transonic flow effects the curves for the different flight-level computations differ strongly. Keep in mind that only at the vertical flight-level lines the result is accurate. This means, if flutter process 1 (FP1) is followed, the error in the GAF-matrix increases with increasing difference of current p-k-method flight level to the GAF-computation flight level. Most conservative is here to pick a small flight level which is connected to a lower lift coefficient and a lower angle of attack. However, often unsteady aerodynamic forces increase with the angle of attack until flow separation occurs. Hence, there is no obvious selection of conservative flight conditions.

Overall, the section shows that for higher Mach-numbers it is not sufficient to use only one aerodynamic dataset for one Mach-number.

5.3 Nonlinear CSM

In this section the fidelity is increased further. For the same cases the already seen flutter-process (FP2) is compared to the result with flutter process 3 (FP3). This means, for FP3 for

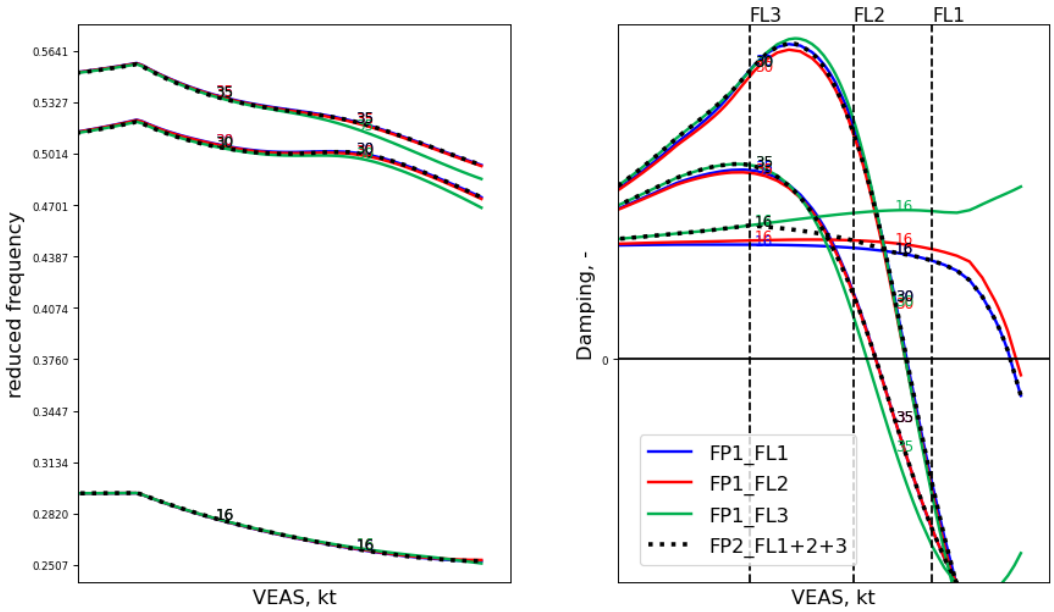

Figure 7: Flutter results flutter process (FP) 1+2 for low Mach-number, 1.7 G maneuvre: Linear CSM, FP1 for 3 flight levels (FL), FP2 with GAF interpolation of same GAF data

each flight-level also the changes in mode-shapes and eigenfrequencies are taken into account. It can be noted that for the low Mach-number, low lift result in Figure 10 differences are visible between FP2 and FP3. The nonlinear process shows the more critical result. Furthermore it can be seen that the mass and stiffness matrix interpolation changes the results only slightly. This is also visible in the small changes in the eigenfrequencies for most eigenmodes. Since no big influences of the steady and unsteady aerodynamics on this case were visible (Figure 6), these differences show the influence of the geometric nonlinear structural modelling. A

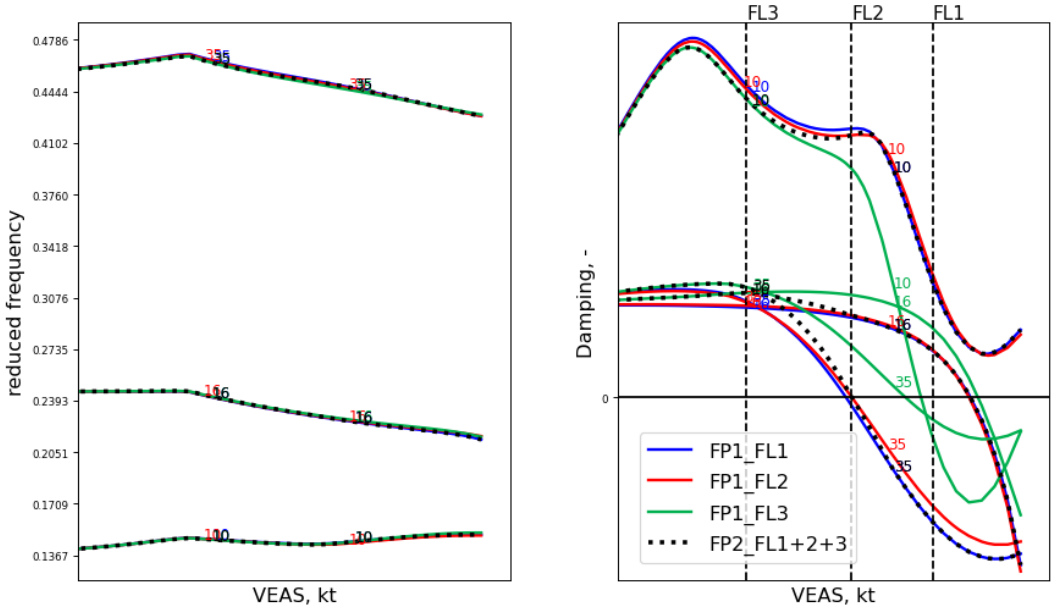

Figure 8: Flutter results flutter process (FP) 1+2 for medium, transonic Mach-number: Linear CSM, FP1 for 3 flight levels (FL), FP2 with GAF interpolation of same GAF data

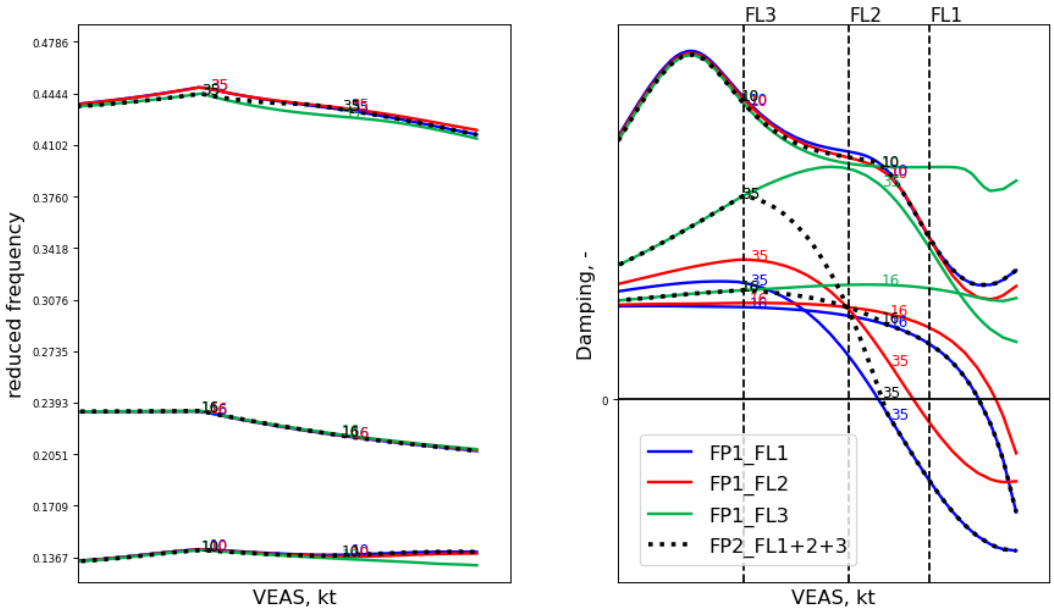

Figure 9: Flutter results flutter process (FP) 1+2 for higher, transonic Mach: Linear CSM, FP1 for 3 flight levels (FL), FP2 with GAF interpolation of same GAF data

similar picture is visible for the 1.7G case in Figure 11. Due to the increased wing deformation the differences of structural linear and nonlinear workflow increase further, leading to an even more critical flutter speed for the flutter process 3.

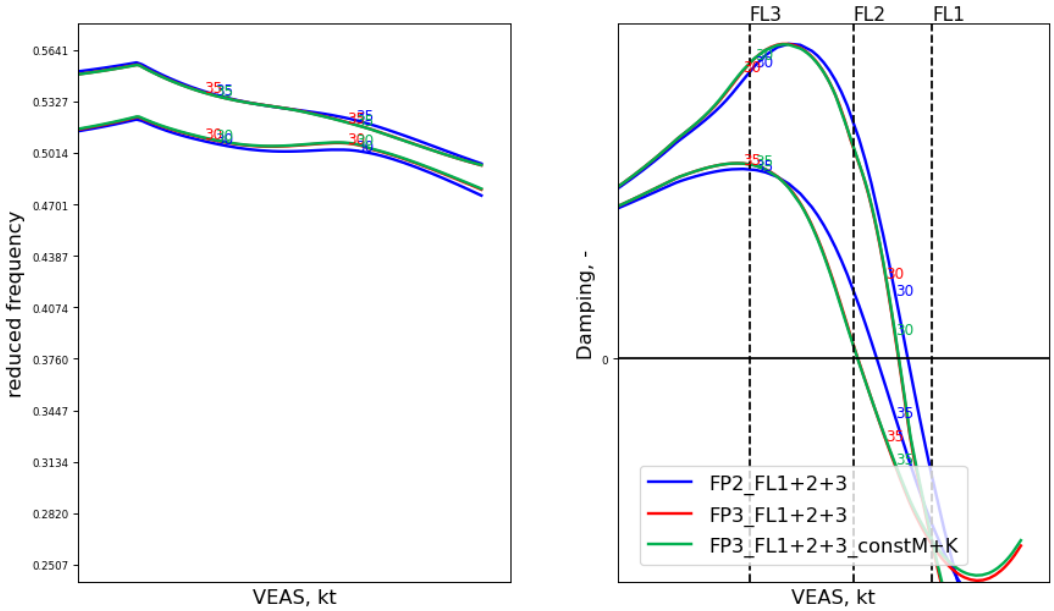

Figure 10: Flutter results flutter process (FP) 2+3 for low Mach-number: FP2 with GAF-interpolation, FP3 with mode-set $\mathbf{\Phi}$ dependent GAF and mass $\mathbf{M}$ + stiffness $\mathbf{K}$ interpolation, additionally FP3 with constant $\mathbf{M}$ and $\mathbf{K}$

For the medium Mach-number the differences between the two workflows are similar for two of the depicted flutter couplings, see Figure 12. As already seen for the low-Mach-number results, the nonlinear FP3 shows more critical results. A similar trend is visible in Figure 13 for the high Mach-number. The change in flutter speed due to the nonlinear flutter process 3 are similar.

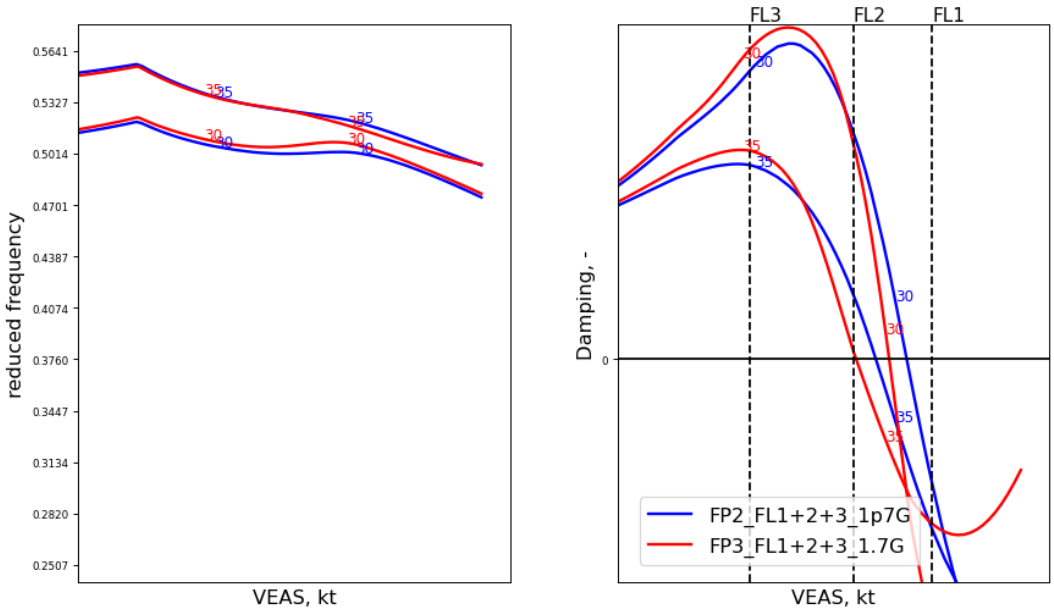

Figure 11: Flutter results flutter process (FP) 2+3 for low Mach-number, 1.7 G maneuvre: FP2 with GAF-interpolation, FP3 with mode-set Φ dependent GAF and mass + stiffness interpolation

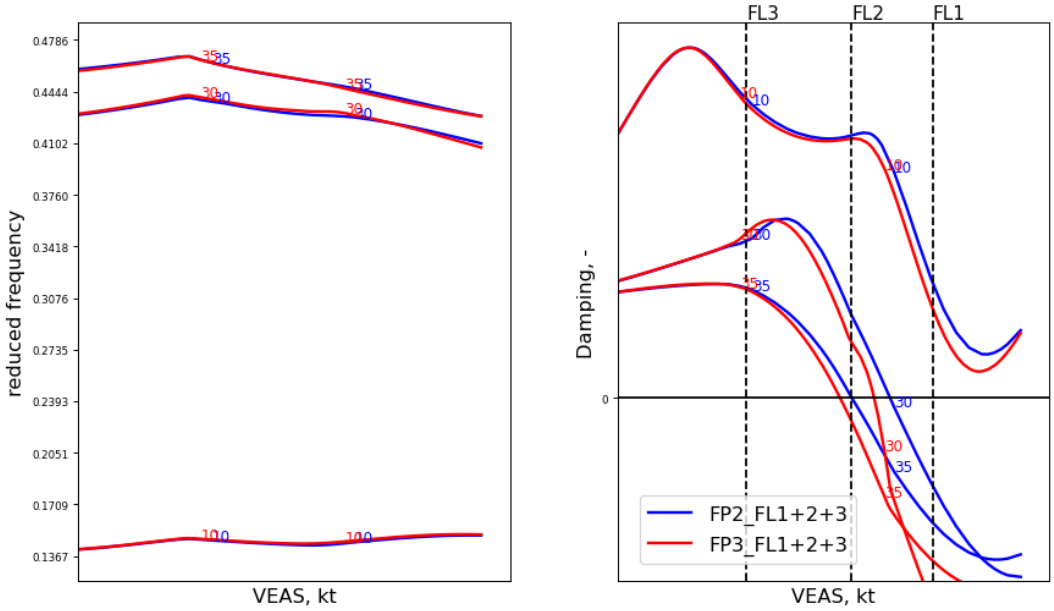

Figure 12: Flutter results flutter process (FP) 2+3 for medium, transonic Mach-number: FP2 with GAF-interpolation, FP3 with mode-set Φ dependent GAF and mass + stiffness interpolation

Concerning the developed method, it should be mentioned that the damping curves are sometimes not very smooth. Here further investigations might be necessary to achieve smoother results between the data points. The question if this is a problem of the method itself or an interpolation problem cannot be solved here.

6 CONCLUSION AND OUTLOOK

The paper shows the importance of flight-condition dependent flutter analysis for a relatively flexible high-aspect ratio wing. Two flutter methods with speed-dependent interpolation of

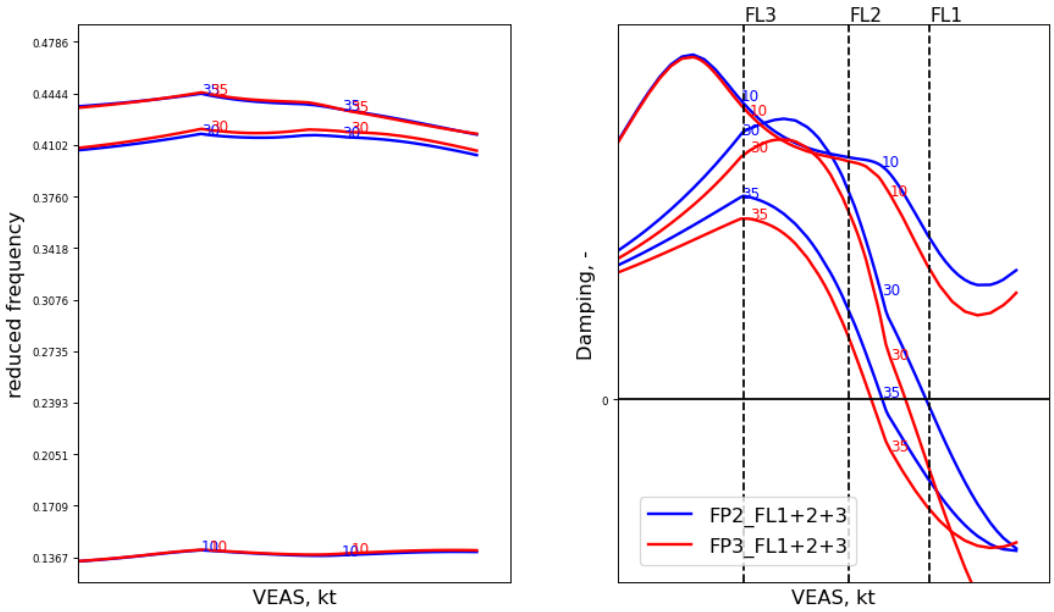

Figure 13: Flutter results flutter process (FP) 2+3 for higher, transonic Mach: FP2 with GAF-interpolation, FP3 with mode-set Φ dependent GAF and mass + stiffness interpolation

generalised aerodynamic and structural matrices have been introduced. This overcomes the problem that not all flight-conditions could be computed with CFD due to excessive computation costs. Instead, relatively simple spline-interpolation methods are used. For a selection of flutter couplings for a generic full-aircraft test-case the methods were compared. It is shown that different steady aerodynamics for different flight-levels lead to strongly differing flutter results. Furthermore, when also the structural model was deformed to the according flight-level shape, further differences were found. These geometric nonlinear effects are not neglectable. It has been shown that these differences increase with the amount of wing-tip deformation. The presented results show for all Mach-numbers an in creasing criticality for the nonlinear flutter process.

With the presented method further studies could be performed: How well do the interpolated flutter results fit to actual test computations in the interpolation range? How must the method be updated to achieve better agreement or smoother result curves?

7 REFERENCES

[1] Ting, E., Reynolds, K., Nguyen, N., et al. (2014). Aerodynamic analysis of the truss-braced wing aircraft using vortex-lattice superposition approach. doi:10.2514/6.2014-2597.

[2] Patil, M. and Hodges, D. (2004). On the importance of aerodynamic and structural geometrical nonlinearities in aeroelastic behavior of high-aspect-ratio wings. *Journal of Fluids and Structures*, 19(7), 905–915. ISSN 0889-9746. doi:https://doi.org/10.1016/j.jfluidstructs.2004.04.012.

[3] Hermanutz, A. and Hornung, M. In *International Forum on Aeroelasticity and Structural Dynamics*.

[4] Stickan, B. (2018). *Explanation of AEROSTABIL limit-cycle oscillations via high-fidelity aeroelastic simulations*. Ph.D. thesis.

[5] Hassig, H. J. (1971). An approximate true damping solution of the flutter equation by determinant iteration. *Journal of Aircraft*, 8(11), 885–889.

[6] Thormann, R. and Widhalm, M. (2013). Linear-Frequency-Domain Predictions of Dynamic-Response Data for Viscous Transonic Flows. *AIAA Journal*, 51(11).

[7] Barnewitz, H. and Stickan, B. (2013). Improved mesh deformation. In B. Eisfeld, H. Barnewitz, W. Fritz, and F. Thiele (Eds.), *Management and Minimisation of Uncertainties and Errors in Numerical Aerodynamics*, vol. 122 of *Notes on Numerical Fluid Mechanics and Multidisciplinary Design*. Springer Berlin Heidelberg. ISBN 978-3-642-36184-5, pp. 219–243.

[8] B. Stickan, R. T., S. VimalKumar (2022). Multi-level meshing strategy for aeroelastic, frequency domain cfd application. In *International Forum on Aeroelasticity and Structural Dynamics*. Madrid, Spain. IFASD-2022-17.

COPYRIGHT STATEMENT